Interplay of 95 GeV diphoton excess and dark matter in supersymmetric triplet model*

Zetian Li (李泽田)[1] Ning Liu (刘宁)[2†] Bin Zhu (祝斌)[1‡]

[1]Department of Physics, Yantai University, Yantai 264005, China
[2]Department of Physics and Institute of Theoretical Physics, Nanjing Normal University, Nanjing 210023, China

Abstract: The decay of the Higgs boson and the nature of dark matter remain fundamental challenges in particle physics. We investigate the 95 GeV diphoton excess and dark matter within the framework of the triplet-extended minimal supersymmetric standard model (TMSSM). In this model, an additional hypercharge $Y=0$, $SU(2)_L$ triplet superfield is introduced. Mixing between the triplet and doublet Higgs states enhances the diphoton signal strength of the 95 GeV Higgs boson, resulting in $\mu_{\gamma\gamma}^{\rm CMS+ATLAS}=0.24^{+0.09}_{-0.08}$, which is consistent with experimental observations. This enhancement arises primarily from charged Higgs and chargino loop contributions, together with an LEP excess in the $Zb\bar{b}$ channel around the same mass within the 2σ range. Additionally, the model accommodates viable dark matter candidates in the form of a bino-dominated neutralino. The relic density is reduced to the observed value through resonance-enhanced annihilation via the Higgs portal or co-annihilation with the triplino or higgsino. This reduction remains consistent with constraints from direct and indirect detection experiments. A comprehensive parameter scan demonstrates that the TMSSM can simultaneously explain the 95 GeV diphoton excess, observed 125 GeV Higgs mass, and dark matter relic density, establishing a compelling and theoretically consistent framework.

Keywords: diphoton excess, Higgs resonance, dark matter

DOI: 10.1088/1674-1137/ae1373 **CSTR:** 32044.14.ChinesePhysicsC.50023110

I. INTRODUCTION

The standard model (SM) of particle physics, a cornerstone of our understanding of fundamental interactions, faces significant challenges in explaining the hierarchy problem of Higgs boson mass and the nature of dark matter (DM). The SM cannot stabilize the Higgs mass against quantum corrections, a deficiency known as the hierarchy problem [1, 2], which results in sensitivity to ultraviolet (UV) divergences. Supersymmetry [3, 4] offers a compelling solution by introducing supersymmetric partners that cancel quadratic loop corrections, thereby stabilizing the Higgs mass and reducing fine-tuning. The lightest supersymmetric particle (LSP), stabilized by R-parity, serves as a natural DM candidate, often identified as the neutralino [5, 6].

The discovery of the 125 GeV Higgs boson by ATLAS and CMS has profound implications for supersymmetric models. Reproducing $m_h=125$ GeV in the minimal supersymmetric SM (MSSM) requires stops well above the current LHC reach, thereby reintroducing fine-tuning [7, 8]. This tension is known as the "little hierarchy problem" [9]. The triplet-extended MSSM (TMSSM) [10−23] potentially resolves this challenge by introducing an $SU(2)_L$ triplet superfield. This addition enhances the Higgs quartic coupling at the tree level through an additional F-term contribution [24], enabling a 125 GeV Higgs mass with sub-TeV stops and significantly reducing fine-tuning.

Recent data from CMS [25, 26] and ATLAS [27, 28] have indicated a significant signal for a 95 GeV Higgs boson decaying to diphotons. CMS observed a local excess with a significance of 2.9σ and a signal strength of $\mu_{\gamma\gamma}=0.33^{+0.19}_{-0.12}$, whereas ATLAS observed $\mu_{\gamma\gamma}=0.18\pm0.10$. The combined signal strength, $\mu_{\gamma\gamma}^{\rm CMS+ATLAS}=0.24^{+0.09}_{-0.08}$ [29], suggests that the 95 GeV Higgs may exceed the SM prediction, indicating potential new physics. Similarly, the LEP collaboration reported an excess in Higgs boson

Received 26 August 2025; Accepted 14 October 2025; Accepted manuscript online 15 October 2025

* Supported by the National Natural Science Foundation of China (NNSFC) (12275232, 12335005) and Bin Zhu is also supported by the Natural Science Foundation of Shandong Province (ZR2025QA20)

† E-mail: liuning@njnu.edu.cn
‡ E-mail: zhubin@mail.nankai.edu.cn

decays to $b\bar{b}$ pairs within the same mass range [30], with a measured signal strength of $\mu^{\rm exp}_{b\bar{b}} = 0.117 \pm 0.057$. These complementary observations suggest a possible common origin in new physics.

Triplet-extended models introduce an $SU(2)_L$ triplet scalar field, which can explain the 95 GeV diphoton excess through mixing with the SM Higgs doublet, enhancing the diphoton decay rate. This mechanism has been extensively studied in non-supersymmetric frameworks [29, 31−65], where the precise tuning of triplet-doublet mixing and mass splittings between charged and neutral Higgs states amplifies the diphoton signal strength while satisfying experimental constraints. In supersymmetry, the singlet-extended MSSM has also been thoroughly investigated [66−81]. Given this promising property, it is compelling to explore whether the TMSSM, the supersymmetric generalization, retains this feature. In the TMSSM, supersymmetry imposes strict relations on coupling constants, avoiding the artificial adjustments often required in non-supersymmetric models. This rigidity may preserve the enhanced diphoton signal necessary to explain the 95 GeV excess while eliminating the need for fine-tuning couplings, offering a significant advantage over non-supersymmetric approaches.

Additionally, the triplet Higgs field introduces new annihilation channels for neutralinos [21], particularly when the triplet mass is approximately twice that of the neutralino, approximately 95 GeV or 125 GeV. The triplino, the supersymmetric partner of the triplet Higgs, is key to neutralino annihilation. We demonstrate that, even if the triplino is not the LSP, it can significantly influence DM annihilation by modifying chargino masses. This modification substantially alters the DM relic density through bino-triplino co-annihilation processes [82].

In this study, we show that the TMSSM simultaneously accounts for the 95 GeV diphoton excess and the DM phenomenology. Through a detailed analysis of the Higgs and neutralino sectors and a comprehensive parameter scan, we identify viable parameter regions that satisfy all relevant constraints, presenting a compelling extension of the SM.

The remainder of this paper is structured as follows: Section II presents the TMSSM framework, focusing on the impact of the $SU(2)_L$ triplet superfield on the Higgs sector. We analytically demonstrate how the triplet accounts for the 95 GeV Higgs and its diphoton excess. Section III explores the roles of the triplet and triplino in DM phenomenology, analyzing their effects on annihilation cross-sections and relic density while ensuring consistency with detection constraints. Section IV evaluates the ability of the TMSSM to simultaneously address the Higgs decay and DM problems through a comprehensive parameter scan. Section V summarizes the findings and discusses their broader implications for physics beyond the SM.

II. HIGGS SECTOR: HIGGS MASS AND ITS DECAY

The TMSSM extends the MSSM through the introduction of an additional $SU(2)_L$-triplet superfield Σ:

$$\Sigma = \begin{pmatrix} T^0/\sqrt{2} & T^+ \\ T^- & -T^0/\sqrt{2} \end{pmatrix}. \tag{1}$$

The TMSSM superpotential adds two terms: a triplino mass term μ_T and a cubic coupling λ that mixes the triplet with the Higgs doublets. The full superpotential reads

$$W_{\rm TMSSM} = W_{\rm MSSM} + \lambda H_u \cdot \Sigma H_d + \mu_T {\rm Tr}\Sigma^2. \tag{2}$$

The model also incorporates soft SUSY-breaking terms:

$$\begin{aligned}\mathcal{L}_{\rm soft} = \mathcal{L}_{\rm MSSM_{SB}} + m_T^2 {\rm Tr}\left(\Sigma^\dagger \Sigma\right) + B_{\mu_T} {\rm Tr}\left(\Sigma^2\right) \\ + T_\lambda H_u \cdot \Sigma H_d + \text{ h.c. },\end{aligned} \tag{3}$$

where only triplet-specific terms are explicitly listed. To simplify the analysis, we choose a SUSY-breaking scale M_S to unify the soft masses $M_S = m_{\tilde{Q}} = m_{\tilde{u}} = m_{\tilde{d}} = m_{\tilde{L}} = m_{\tilde{e}}$ and A_0 to represent the trilinear soft terms $A_0 = A_u = A_d = A_e$. The remaining soft masses $m^2_{H_u}$, $m^2_{H_d}$, and m^2_T are determined by imposing the conditions for successful electroweak symmetry breaking (EWSB), *i.e.*, the tadpole equations $\partial V/\partial\phi_i = 0$, where i corresponds to H_u, H_d, and T.

During the EWSB process, the neutral component T^0 of the triplet acquires a vacuum expectation value (VEV). The neutral components of the Higgs doublets and the triplet can be expressed as fluctuations around their respective VEVs:

$$\begin{aligned} H_d^0 &= \frac{1}{\sqrt{2}}(v_d + \phi_d + {\rm i}\sigma_d), \\ H_u^0 &= \frac{1}{\sqrt{2}}(v_u + \phi_u + {\rm i}\sigma_u), \\ T^0 &= \frac{1}{\sqrt{2}}(v_T + \phi_T + {\rm i}\sigma_T), \end{aligned} \tag{4}$$

where v_d, v_u, and v_T are the VEVs of the Higgs doublets and the triplet, respectively. ϕ_d, ϕ_u, and ϕ_T represent their real parts, and σ_d, σ_u, and σ_T denote their imaginary parts.

The electroweak scale is defined by the Higgs VEVs as $v = \sqrt{v_d^2 + v_u^2} = 246$ GeV. Triplet-extended models face constraints from electroweak precision tests (EWPT), particularly through the ρ parameter. A non-zero triplet VEV v_T alters ρ from unity according to $\rho = 1 + \dfrac{4v_T^2}{v^2}$. The experimental value $\rho = 1.0004^{+0.0003}_{-0.0004}$ limits $v_T \lesssim 4$ GeV. However, introducing two additional triplet chiral superfields with hypercharges $Y = \pm 1$, alongside the $Y = 0$ triplet, preserves custodial symmetry in the superpotential [83]. This ensures $\rho = 1$ at the tree level, permitting a larger triplet VEV v_T while remaining consistent with EWPT constraints.

The mixing between different gauge eigenstates (ϕ_d, ϕ_u, ϕ_T) results in the formation of a non-diagonal CP-even Higgs mass matrix:

$$\mathcal{M}_h^2 = \begin{pmatrix} \mathcal{M}_{\phi_d\phi_d} & \mathcal{M}_{\phi_u\phi_d} & \mathcal{M}_{\phi_T\phi_d} \\ \mathcal{M}_{\phi_d\phi_u} & \mathcal{M}_{\phi_u\phi_u} & \mathcal{M}_{\phi_T\phi_u} \\ \mathcal{M}_{\phi_d\phi_T} & \mathcal{M}_{\phi_u\phi_T} & \mathcal{M}_{\phi_T\phi_T} \end{pmatrix}. \tag{5}$$

The mass matrix is diagonalized by a unitary matrix Z_H:

$$Z^H \mathcal{M}_h^2 Z^{H\dagger} = m_h^{\rm dia}, \tag{6}$$

where its elements relate the gauge eigenstates to the mass eigenstates:

$$h_i = Z^H(i,1)\phi_d + Z^H(i,2)\phi_u + Z^H(i,3)\phi_T, \tag{7}$$

This allows us to track the contribution of each gauge eigenstate to the physical Higgs states through the Z^H matrix during the calculation.

Within the limits of a small v_T and λ, the triplet sector almost decouples from the doublet sector. Consequently, the 95 GeV Higgs predominantly originates from the triplet itself. Therefore, we analyze the (33)-th component of the mass matrix first and denote the lightest Higgs mass by m_h:

$$m_h^2 = \mathcal{M}_{\phi_T\phi_T} = 2B_{\mu_T} + 4\mu_T^2 + m_T^2, \tag{8}$$

where m_T^2 can be determined by solving the tadpole equations at the EWSB scale $\partial V/\partial\phi_T = 0$:

$$\begin{aligned} m_T^2 = & -2B_{\mu_T} - 4\mu_T^2 + \frac{\lambda}{2}\left(\frac{v}{v_T}\right) v\mu_T \sin(2\beta) \\ & - \frac{\lambda}{4}\left(\frac{v}{v_T}\right) v\mu \sin^2\beta, \end{aligned} \tag{9}$$

This relation holds exclusively at the tree level, neglecting terms linear in λ and v_T. However, we note that a linear term in λ persists in Eq. (9) owing to the v/v_T enhancement, which counteracts the λ suppression. By substituting m_T^2 from Eq. (9) into the triplet Higgs mass (Eq. (8)), we observe a precise cancellation of B_{μ_T}:

$$m_h^2 = \frac{\lambda}{2}\left(\frac{v}{v_T}\right) v\mu_T \sin(2\beta) - \frac{\lambda}{4}\left(\frac{v}{v_T}\right) v\mu \sin^2\beta. \tag{10}$$

This cancellation explains the independence of the lightest Higgs boson mass on B_{μ_T} in Fig. 1 (left panel). The residual minor dependence on B_{μ_T} arises from loop-level corrections.

The right panel of Fig. 1 shows that the mass of the triplet-dominated lightest Higgs is inversely proportional to μ_T, which appears to contradict the linear dependence on μ_T predicted by Eq. (10). This apparent contradiction is resolved by the negative cubic coupling λ, which reverses the proportionality. Consequently, the lightest Higgs mass scales inversely with μ_T, as depicted in Fig. 1. We numerically exclude the light-gray region where the squared mass of the charged Higgs, $m_{H^\pm}^2$, is negative.

The doublet Higgs is responsible for the observed 125 GeV Higgs boson. The tree-level Higgs mass enhancement, proportional to $\lambda^2 v^2 \sin^2 2\beta$, is suppressed owing to the small value of λ. Therefore, we rely on a high supersymmetry (SUSY) scale and large trilinear couplings to achieve the required Higgs mass. The left panel in Fig. 2 illustrates that maximal mixing ($A_0 \sim M_S$) considerably enhances the Higgs mass, avoiding the need for very large M_S values. When A_0 is small, the Higgs mass depends more on the SUSY scale M_S, requiring larger M_S for higher Higgs boson masses.

The right panel in Fig. 2 provides an enlarged view of the purple region in the right panel in Fig. 1. Although the triplet sector is nominally decoupled, the triplet parameter μ_T still affects the mass of the SM Higgs boson. Direct inspection shows that the $\mathcal{M}_{\phi_d\phi_d}$ and $\mathcal{M}_{\phi_u\phi_u}$ mass matrix components depend on μ_T through the highly suppressed term $\lambda v_T/v$, allowing these contributions to be safely neglected. The μ_T dependence instead arises from the off-diagonal mixing terms $\mathcal{M}_{\phi_u\phi_T}$ and $\mathcal{M}_{\phi_d\phi_T}$. For example, the $\mathcal{M}_{\phi_u\phi_T}$ component is

$$\mathcal{M}_{\phi_u\phi_T} = -\lambda v(\mu_T \cos\beta - \mu \sin\beta) + O(\lambda^2). \tag{11}$$

Despite $\lambda \sim O(-0.1)$, its residual contribution induces a measurable shift in the 95 and 125 GeV Higgs boson masses. The mixing between the doublet and triplet Higgs fields $h = \phi_{\rm SM}\cos\theta + \phi_T \sin\theta$ is essential for producing the lightest neutral Higgs boson via gluon fusion. Without this mixing, gluon fusion —the dominant production mechanism—would be absent, as the triplet Higgs does not couple directly to fermions.

Alternative processes, such as vector boson fusion or associated production, typically yield insufficient cross-sections. Thus, doublet-triplet mixing is necessary to achieve a sufficiently large production cross-section via gluon fusion, explaining the observed diphoton excess, which is determined as follows,

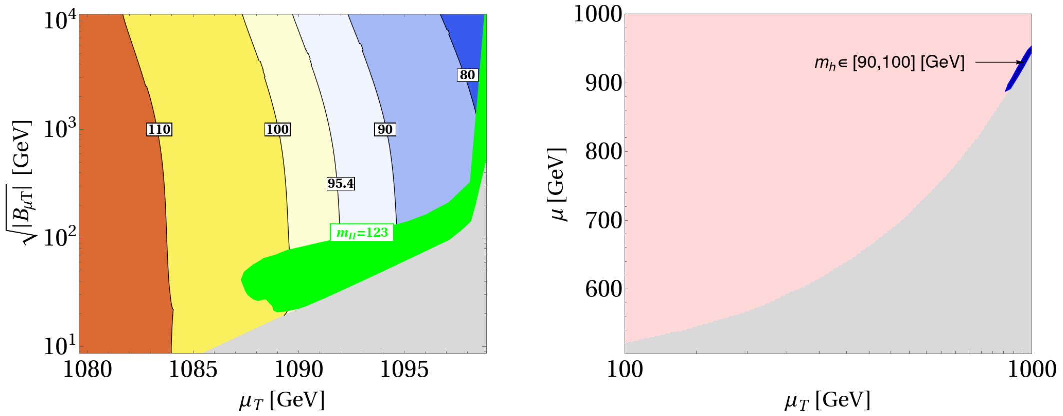

Fig. 1. (color online) Left: Contour plot of the lightest Higgs mass m_h in the $\sqrt{B_{\mu_T}}-\mu_T$ parameter space, with $\mu = 1$ TeV, $M_S = 5.01$ TeV, $A_0 = 12$ TeV; the green region shows the SM Higgs mass below 123 GeV. Right: Contour plot of the lightest Higgs boson mass m_h in the $\mu-\mu_T$ parameter space, with $M_S = 5.01$ TeV, $A_0 = 12$ TeV, and $\sqrt{B_{\mu_T}} = \sqrt{5}$ TeV.

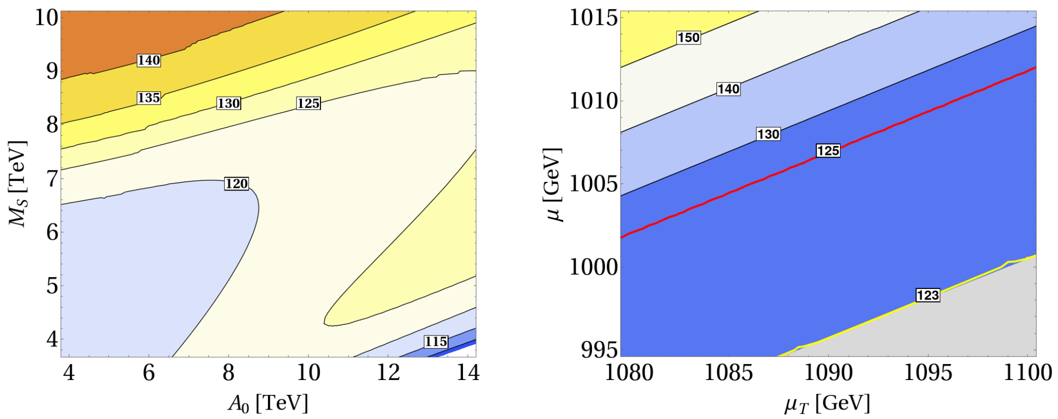

Fig. 2. (color online) Left: Contour plot of the SM Higgs mass m_H in the A_0-M_S parameter space, with $\mu = 1$ TeV, $\mu_T = 1.092$ TeV, and $B_{\mu_T} = 5\,(\text{TeV})^2$. Right: Contour plot of the SM Higgs boson mass m_H in the $\mu-\mu_T$ parameter space, with $M_S = 5.01$ TeV, $A_0 = 12$ TeV, and $B_{\mu_T} = 5\,(\text{TeV})^2$.

$$\mu_{\gamma\gamma} = \frac{\sigma_{\rm SUSY}(pp\to h)\times {\rm Br}_{\rm SUSY}(h\to\gamma\gamma)}{\sigma_{\rm SM}(pp\to h)\times {\rm Br}_{\rm SM}(h\to\gamma\gamma)}. \tag{12}$$

To influence $\mu_{\gamma\gamma}$, modifications to either the Higgs production mechanism or its decay width are required. Owing to the small doublet-triplet mixing angle θ, the gluon fusion production cross-section remains significant, analogous to the SM mechanism. The gluon fusion cross-section for h is

$$\sigma_{ggF} \propto |\cos\theta\cdot A_t(\tau_t) + A_{\tilde t}(\tau_{\tilde t})|^2, \tag{13}$$

where $A_t(\tau_t) = \frac{3}{2}\tau_t\left[1+(1-\tau_t)f(\tau_t)\right]$ (top quark loop) and $A_{\tilde t}$ (stop loop) are loop functions with $\tau_i = 4m_i^2/m_h^2$. The SM cross-section is $\sigma_{ggF}^{\rm SM} \propto |A_t^{\rm SM}|^2$, yielding the ratio

$$\frac{\sigma_{\rm SUSY}}{\sigma_{\rm SM}} = \frac{\sigma_{ggF}}{\sigma_{ggF}^{\rm SM}} = \left|\cos\theta + \frac{A_{\tilde t}}{A_t^{\rm SM}}\right|^2 \sim 1. \tag{14}$$

For small mixing and large SUSY scale M_S, the production cross-section ratio approaches the SM. Thus, deviations in the diphoton signal arise predominantly from the decay width. In the SM, the diphoton decay rate of the Higgs boson is expressed as

$$\Gamma(h\to\gamma\gamma) = \frac{G_\mu\alpha^2 m_h^3}{128\sqrt{2}\pi^3}\left|\sum_f N_c Q_f^2 A_{1/2}^h(\tau_f) + A_1^h(\tau_W)\right|^2, \tag{15}$$

In the TMSSM, the diphoton decay rate [84] is modified to

$$\begin{aligned}\Gamma(h\to\gamma\gamma) = \frac{G_\mu\alpha^2 m_h^3}{128\sqrt{2}\pi^3}\Bigg|&\sum_f N_c Q_f^2 g_{hff} Q_V^2 A_{1/2}^h(\tau_f) \\ &+ g_{hVV}A_1^h(\tau_W) + \frac{M_W^2\lambda_{hH^+H^-}}{2c_W^2 m_{H^\pm}^2}A_0^h(\tau_{H^\pm}) \\ &+ \mathcal{A}_{\rm SUSY}^h\Bigg|^2,\end{aligned} \tag{16}$$

It describes the effective coupling of the light Higgs to diphotons, incorporating both the SM and new supersymmetric contributions. The amplitude $\mathcal{A}^h_{\rm SUSY}$ shares the same structure as the SM except the loop particle being a SUSY partner. Compared with the SM, our setup includes two key additional contributions that modify the $h\to\gamma\gamma$ partial width. The first is a loop contribution from the charged Higgs bosons arising from the triplet scalar. The second is from the charginos. Both contributions lead to an enhancement in the diphoton rate.

The loop functions are defined as follows:

- $A^h_1(\tau) = -\left(2\tau^2+3\tau+3(2\tau-1)f(\tau)\right)\tau^{-2}$, the loop function for the W-boson.

- $A^h_0(\tau) = -\left[\tau - f(\tau)\right]\tau^{-2}$, the loop function for the scalar particles.

- $A^h_{1/2}(\tau) = 2\left(\tau+(\tau-1)f(\tau)\right)\tau^{-2}$, the loop function for the fermions.

These loop functions reveal that additional contributions from charged Higgs bosons and charginos modify the Higgs decay width. For charginos, although heavier masses would naively induce larger deviations, their contribution is suppressed by the loop function $A_{1/2}(\tau_{\chi^\pm})$. This interplay naturally prevents the unphysical growth of deviations while maintaining consistency with the decoupling theorem. Thus, the dominant contribution arises from the lightest charged Higgs boson (charged triplet) and moderate chargino mass, as numerically verified in Section IV.

The normalized $b\bar{b}$ signal strength at 95.4 GeV is defined relative to a benchmark hypothetical SM Higgs boson of the same mass [71]:

$$\mu_{b\bar{b}} = \frac{\sigma_{\rm SUSY}(e^+e^-\to Zh)\times {\rm Br}_{\rm SUSY}(h\to b\bar{b})}{\sigma_{\rm SM}(e^+e^-\to Zh)\times {\rm Br}_{\rm SM}(h\to b\bar{b})}. \tag{17}$$

Here, the SM quantities in the denominator are calculated for a scalar with $m_h = 95.4$ GeV and SM-like couplings. The observed signal strength of $b\bar{b}$ near 95 GeV is consistent with zero (Fig. 3). The shaded blue band indicates the 1σ region for $\mu_{\gamma\gamma}$, whereas the light - blue envelope shows its 2σ extension. Similarly, the dark - red band represents the 1σ interval for the $b\bar{b}$ channel, and the pale - red shading corresponds to the 2σ bounds. The light-green strip highlights the mass window of $m_h = 95.4\pm1$ GeV. Given that the excess signals observed in the LEP, CMS, and ATLAS near 95 GeV are only valid within this specific range, the constraints on $\mu_{\gamma\gamma}$ and $\mu_{b\bar{b}}$ specifically refer to the mass window of $m_h = 95.4\pm1$ GeV.

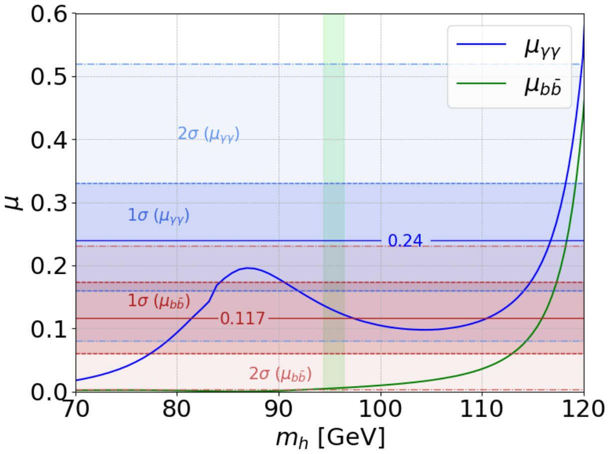

Fig. 3. (color online) Signal strengths of the light scalar Higgs boson decaying into diphoton and bottom quark pairs as a function of its mass with $\mu = 985$ GeV and $\mu_T\in[1000, 1070]$ GeV.

III. NEUTRALINO SECTOR: RELIC DENSITY AND DIRECT DETECTION

The neutralino mass matrix includes the traditional neutralino components: the bino ($\lambda_{\tilde{B}}$), wino ($\tilde{W}^0$), and higgsinos ($\tilde{H}^0_d$, $\tilde{H}^0_u$), as well as the newly introduced fermionic triplet component, the triplino (λ_{T^0}). The specific form of the mass matrix is given as follows:

$$\begin{pmatrix} M_1 & 0 & -\frac{1}{2}g_1 v_d & \frac{1}{2}g_1 v_u & 0 \\ 0 & M_2 & \frac{1}{2}g_2 v_d & -\frac{1}{2}g_2 v_u & 0 \\ -\frac{1}{2}g_1 v_d & -\frac{1}{2}g_2 v_d & 0 & -\frac{1}{2}v_T\lambda-\mu & -\frac{1}{2}v_u\lambda \\ \frac{1}{2}g_1 v_u & -\frac{1}{2}g_2 v_u & -\frac{1}{2}v_T\lambda-\mu & 0 & -\frac{1}{2}v_d\lambda \\ 0 & 0 & -\frac{1}{2}v_u\lambda & -\frac{1}{2}v_d\lambda & 2\mu_T \end{pmatrix}. \tag{18}$$

To investigate the influence of various components on the DM annihilation process, the diagonal process can be employed to study the contribution of the triplino to DM in the TMSSM. First, it is essential to diagonalize the neutralino mass matrix to derive its eigenvalue mass matrix:

$$N^* m_{\tilde{\chi}^0} N^\dagger = m^{\rm dia}_{\tilde{\chi}^0}. \tag{19}$$

The contributions based on the components in the neutralino basis can be expressed as

$$\begin{aligned} &\lambda_{\tilde{B}} = \sum_j N^*_{j1}\lambda^0_j, \quad \tilde{W}^0 = \sum_j N^*_{j2}\lambda^0_j, \quad \tilde{H}^0_d = \sum_j N^*_{j3}\lambda^0_j, \\ &\tilde{H}^0_u = \sum_j N^*_{j4}\lambda^0_j, \quad \lambda_{T^0} = \sum_j N^*_{j5}\lambda^0_j. \end{aligned} \tag{20}$$

We select two benchmark points to examine their contributions to DM composition, as presented in Table 1. These points represent bino-dominated and triplino-dominated DM scenarios. We exclude an explicit discussion of the well-known Higgsino and wino LSP scenarios.

In the parameter selection for ID A, the values are set as follows: $M_1 = 62.5$ GeV $\ll M_2, \mu, \mu_T$, and $\lambda = -0.1$. Specifically, the choice of M_1 aligns the bino mass precisely with the Higgs resonance region, significantly enhancing the annihilation efficiency via s-channel Higgs exchange.

In Fig. 4, the blue curve depicts the neutralino relic density, and the orange line indicates the observed DM relic density, $\Omega h^2 = 0.12$. The green dashed line shows the lightest neutralino mass, which increases linearly with M_1, confirming its dominant bino composition. The bino relic density typically exceeds $\Omega h^2 = 0.12$, but two resonant regimes—where $2m_{\tilde{B}} \approx m_h$ or $2m_{\tilde{B}} \approx m_H$— enable resonant annihilation, sharply reducing the relic density. Additionally, when the cyan dashed line (chargino mass) nears the bino mass, co-annihilation processes further decrease the relic density.

In the TMSSM, the interplay between the DM and the 95 GeV di-photon excess is realized by two mechanisms. First, the triplino–triplet Higgs portal is governed by the supersymmetric mass parameter μ_T, demanding that the triplino $\widetilde{T}$ both be the LSP and reproduce the observed thermal relic abundance forces $\mu_T \sim m_{\widetilde{T}} \gtrsim 1$TeV, at which point the lightest chargino instead becomes the LSP and the simplest μ_T-driven scenario is excluded. Second, a resonant bino–Higgs portal emerges when the bino mass satisfies $m_{\widetilde{B}} \simeq 47.5$ GeV; therefore, the resonant annihilation can both account for the di-photon signal and deplete the relic density. As shown in Fig. 4, although the resonance enhances $\langle\sigma v\rangle$, one finds $\langle\sigma v\rangle_{\rm res} < \langle\sigma v\rangle_{\rm therm}$, leaving an overabundance that a late-time entropy injection can dilute [85] (The relic density in Fig. 4 is computed using MicrOmegas v6.1.15 [86–91]). Thus, while the direct μ_T–mediated triplino mechanism is ruled out, resonant bino annihilation via the 95 GeV Higgs remains a viable link between DM and the di-photon excess.

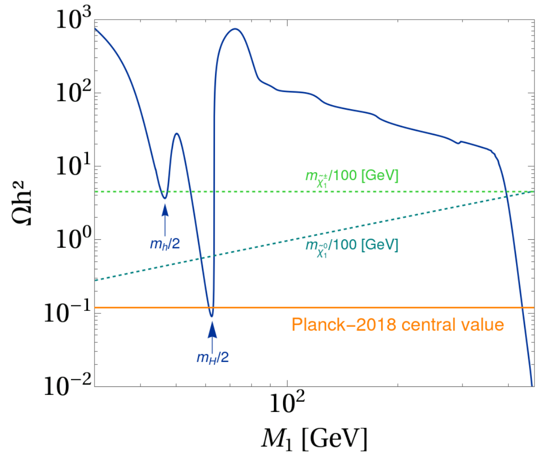

Fig. 4. (color online) The blue solid line is the neutralino relic density with the variation of M_1. The orange solid line is used to highlight the central relic density value from the Planck 2018 data. The green dashed line and cyan dashed line correspond to the lightest chargino and lightest neutralino mass, respectively. The input parameters are set as follows: $\tan\beta = 3.95$, $M_S = 5$ TeV, $\lambda = -0.133$, $\mu_T = 200$ GeV, $\mu = 1$ TeV, $B_{\mu_T} = 5\,({\rm TeV})^2$.

Therefore, analyzing the neutralino mixing matrix Z_N alone is insufficient to fully characterize the role of the triplet sector in DM physics. As evidenced in Fig. 4, bino–chargino co-annihilation processes significantly enhance the DM annihilation cross-section [92–95]. Therefore, a complete analysis requires the inclusion of the chargino mass matrix, defined in the basis $\left(\tilde{W}^-, \tilde{H}_d^-, \lambda_{T^-}\right)$ and $\left(\tilde{W}^+, \tilde{H}_u^+, \lambda_{T^+}\right)$. The chargino mass matrix is,

$$m_{\tilde{\chi}^-} = \begin{pmatrix} M_2 & \frac{1}{\sqrt{2}} g_2 v_u & -g_2 v_T \\ \frac{1}{\sqrt{2}} g_2 v_d & -\frac{1}{2} v_T \lambda + \mu & -\frac{1}{\sqrt{2}} v_u \lambda \\ g_2 v_T & \frac{1}{\sqrt{2}} v_d \lambda & 2\mu_T \end{pmatrix}. \tag{21}$$

Table 1. Composition of bino LSP and triplino as DM and their Z^H. Z^H elements correspond to the CP-even Higgs mixing (Eqs. (6) and (7)), and Z^N elements denote the neutralino mixing components (Eqs. (19) and (20)).

Z^N and Z^H Matrices					
ID A	$Z^N(1,1)$	$Z^N(1,2)$	$Z^N(1,3)$	$Z^N(1,4)$	Ωh^2
	-9.9918×10^{-1}	5.1812×10^{-4}	-3.8790×10^{-2}	1.1637×10^{-2}	0.115
	$Z^N(1,5)$	$Z^H(1,1)$	$Z^H(1,2)$	$Z^H(1,3)$	$\langle\sigma v\rangle$ /cm^3 s^{-1}
	1.6007×10^{-4}	3.4175×10^{-3}	6.0784×10^{-2}	9.9815×10^{-1}	1.8375×10^{-32}
ID B	$Z^N(1,1)$	$Z^N(1,2)$	$Z^N(1,3)$	$Z^N(1,4)$	Ωh^2
	-2.0387×10^{-4}	4.7161×10^{-4}	-2.2499×10^{-2}	1.3659×10^{-2}	5.8860×10^{-4}
	$Z^N(1,5)$	$Z^H(1,1)$	$Z^H(1,2)$	$Z^H(1,3)$	$\langle\sigma v\rangle$ /cm^3 s^{-1}
	9.9991×10^{-1}	1.3531×10^{-2}	6.5181×10^{-2}	9.9778×10^{-1}	2.83×10^{-24}

In the limit of small λ and v_T, the mass matrix becomes nearly diagonal, showing that μ_T governs the charged triplino mass. This parameter also controls the masses of the lightest Higgs boson and triplino, allowing the simultaneous study of Higgs and DM phenomenology through μ_T.

For the bino annihilation, the dominant process in the Higgs resonance region is bino pairs annihilating into bottom quarks via the s-channel exchange of the Higgs boson [96]. This is natural, as the third-generation Yukawa coupling is the most significant. Additionally, bino–chargino co-annihilation processes occur naturally when $\mu_T \approx M_1$, with the dominant channels being $\tilde{\chi}^0_1 + \tilde{\chi}^{\pm}_1 \to Z + W^-$ and $\tilde{\chi}^0_3 + \tilde{\chi}^{\pm}_1 \to Z + W^-$.

In the parameter set ID B, we set $\mu_T = 50\,\text{GeV}$ with $\mu_T \ll M_1, M_2, \mu$, ensuring that the triplino is the LSP. However, the relic density is low, approximately 10^{-4}, owing to strong $SU(2)$ interactions similar to those of the wino, which requires a mass of $\sim 2\,\text{TeV}$ to match the observed relic density. Although a heavy triplino LSP appears viable for DM, Fig. 5 shows that the triplino ceases to be the LSP above $\sim 100\,\text{GeV}$. At the tree level, with $\mu \gg M_1, M_2$, the neutral and charged triplinos are nearly degenerate ($m \approx 2\mu_T$) and dominate the LSP, as shown in Fig. 5. As μ_T increases, loop corrections raise the mass of the neutral triplino more than that of the charged triplino, because the neutral triplino, a Majorana fermion, experiences larger Z-boson and scalar loop effects, whereas the charged triplino, a Dirac fermion, incurs smaller photon and W-boson corrections. This inverts the mass hierarchy, making the charged triplino the LSP. Consequently, we adopt a bino LSP for this study.

We now consider the direct detection of neutralino DM [97], with a dominant bino component as established [98]. The spin-independent scattering cross-section between the neutralino and a nucleus originates from the effective Lagrangian [99],

$$\mathcal{L}_{\text{eff}} = a_q \bar{\chi}^0_1 \chi^0_1 \bar{q} q, \tag{22}$$

where a_q parametrizes the neutralino-quark coupling, and the resulting neutralino-nucleon cross-section becomes

$$\sigma_{\text{SI}} = \frac{4\mu_r^2}{\pi}\left(\sum_{q=u,d,s} f^{(p,n)}_{Tq} a_q \frac{m_{p,n}}{m_q} + \frac{2}{27} f^{(p,n)}_{TG} \sum_{q=c,b,t} a_q \frac{m_{p,n}}{m_q}\right)^2, \tag{23}$$

with μ_r, the neutralino-nucleon reduced mass, and $f^{(p,n)}_{TG} = 1 - \sum_{q=u,d,s} f^{(p,n)}_{Tq}$ and the form factors are $f^{(p)}_{Tu} = 0.020 \pm 0.004$, $f^{(p)}_{Td} = 0.026 \pm 0.005$, $f^{(p)}_{Ts} = 0.118 \pm 0.062$, $f^{(n)}_{Tu} = 0.014 \pm 0.003$, $f^{(n)}_{Td} = 0.036 \pm 0.008$, and $f^{(n)}_{Ts} = 0.118 \pm 0.062$ [100]. The dominant contribution to a_q/m_q originates from t-channel CP-even Higgs exchange, scaling as

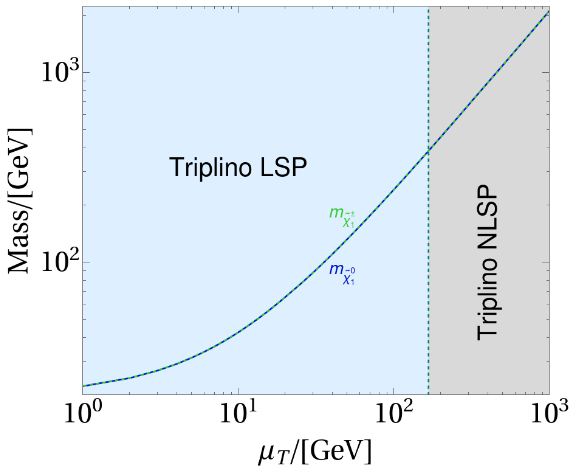

Fig. 5. (color online) Masses of the charged triplino and neutral triplino as a function of μ_T, and the status for the LSP.

$$\frac{a_q}{m_q} \simeq \sum_i \frac{S_{\chi\chi h_i}}{m^2_{h_i}} S_{h_i qq}. \tag{24}$$

For the lightest Higgs with mass $m_h \simeq 95.4\,\text{GeV}$, the coupling is

$$\begin{aligned} S_{\chi\chi h_1} \simeq\ & g_2(Z^N_{12} - \tan\theta_W Z^N_{11})(Z^H_{11} Z^N_{13} - Z^H_{12} Z^N_{14}) \\ & + \lambda(Z^H_{11} Z^N_{15} Z^N_{13} + Z^H_{12} Z^N_{15} Z^N_{14} + Z^H_{13} Z^N_{13} Z^N_{14}), \end{aligned} \tag{25}$$

where Z^N_{ij}, Z^H_{ij}, and λ denote neutralino mixing, Higgs mixing, and model parameters, respectively. Therefore, we obtain the cross-section for ID A as 1.0110×10^{-11} pb, and for ID B as 6.3827×10^{-15} pb.

IV. NUMERICAL RESULT

We constructed the Lagrangian of the model using SARAH v4.15.3 [101] and calculated the particle spectrum, including Higgs-mass loop corrections and diphoton signal strengths, with SPheno v4.0.5 [102, 103]. Theoretical consistency and experimental Higgs constraints were enforced via HiggsTools [104], HiggsBounds-5 [105−111], and HiggsSignals-2 [112−115], whereas the DM relic density and DM-nucleon cross-sections were computed with MicrOmegas v6.1.15 [86−91]. Collider limits were validated through SModelS v3 [116], and the entire workflow was automated using BSMArt v1.5 [117−126]. Fixed parameters were specified and Bayesian parameter estimation was performed using MultiNest v3.12 [127−129] by scanning the free parameter ranges given in Table 2.

Before presenting our results, we define the conditions for the final selected parameter points. In our fixed-order $\overline{\text{DR}}$ spectrum calculation with SARAH and SPheno, including full momentum-dependent one-loop self-energies and dominant two-loop (effective-potential) corrections of $O(\alpha_s\alpha_t)$ and $O(\alpha_t^2)$ as detailed in [130, 131], we adopt the lightest Higgs mass criterion of $94.4\,\text{GeV} \le m_h \le 96.4\,\text{GeV}$, and we similarly require the SM-like Higgs mass to lie within $123\,\text{GeV} \le m_H \le 127\,\text{GeV}$. For Higgs data fitting, we incorporate direct search results for additional Higgs bosons from the LEP, Tevatron, and LHC experiments. The selected parameter points must satisfy result = 1 in HiggsBounds with the HiggsSignal p-value obtained via χ^2 analysis exceeding 0.05 to ensure statistical significance and experimental consistency.

To account for the systematic uncertainties in DM calculations, we adopted an expanded relic density range of $\Omega h^2 \in [0.096, 0.144]$, corresponding to ±20% variations around the Planck-2018 observed cold DM central value $\Omega h^2 = 0.120$ [132]. For direct and indirect detection constraints, we require a DM signal exclusion statistical reliability of $p \ge 0.05$ at the 95% confidence level, whereas collider limits are enforced via the SModelS exclusion ratio criterion $r < 1$ [116].

We additionally require $m_{H^\pm} \in [110, 120]$ GeV on the charged Higgs mass from stau ($\tilde{\tau}$) searches, following the analysis of Ref. [62]. The similar final-state signatures between $\tilde{\tau}^\pm \to \tau^\pm \tilde{\chi}_1^0$ and $H^\pm \to \tau\nu$ decays (for massless neutrinos) allow the reinterpretation of ATLAS stau search results. The current exclusion limits rule out charged triplet scalars below 110 GeV.

The color scheme employed in the scatter plot adheres to the following consistent convention:

- Red points:

$$m_H = 125 \pm 2\,\text{GeV}, \quad m_{H^\pm} \in [110, 120]\,\text{GeV},$$
$$\text{HBresult} = 1, \quad \text{HSpval} \ge 0.05,$$
$$\Omega h^2 = 0.120 \pm 0.024, \quad \text{DMpval} \ge 0.05,$$
$$\text{SModelSr} < 1, \quad \mu_{\gamma\gamma} = 0.24^{+0.18}_{-0.16},$$
$$\mu_{b\bar{b}} = 0.117 \pm 0.114.$$

- Cyan points – Higgs constraints: The SM Higgs mass lies within the experimentally allowed range and satisfies all HB, HS, and SModelS constraints.

- Yellow points – DM constraints: Ωh^2 lies within a ±20% range, the DM p-value satisfies statistical requirements, and SModelSr < 1.

- Gray points: Only SModelSr < 1.

The left panel in Fig. 6 shows that the cyan data points are nearly independent of M_1 because M_1 only affects the bino mass, which plays no role in the Higgs sector. By contrast, the yellow data points display a specific distribution, where the first cluster lies in the Higgs resonance region at $M_1 \approx m_H/2$. The second cluster appears near the TeV energy scale. This pattern matches our earlier findings reported in Fig. 4. In the low-energy Higgs resonance region, the bino mass M_1 is much smaller than the higgsino mass μ and the triplino mass $2\mu_T$. This enables the region to yield a pure bino DM candidate consistent with observational constraints. At the TeV scale, the near degeneracy of $M_1 \sim \mu \sim \mu_T$ facilitates bino-higgsino or bino-triplino coannihilation via gauge-mediated interactions. This configuration boosts the efficiency of annihilation, yielding a correct DM relic density. The diphoton signal strength $\mu_{\gamma\gamma}$ with a central value of 0.24 and the bottom quark pair signal strength $\mu_{b\bar{b}}$ with a central value of 0.117, both within 2σ, reduce the yellow points to fewer red points. Then, we observe that the overall constraint still has survival points touching the correct 95 GeV Higgs band.

Table 2. Parameter space of the TMSSM: Fixed values (top) and scanned ranges (bottom).

Fixed Parameters			
M_S/TeV	5	$\tan\beta$	3.95
A_0/TeV	12	M_2/TeV	1.5
M_3/TeV	3	A_λ/TeV	2
B_{μ_T}/TeV^2	5	B_μ/TeV^2	1
Scanned Parameter Ranges			
M_1/GeV	(45, 1200)	λ	(–0.3, 0.3)
μ_T/GeV	(500, 2000)	μ/GeV	(500, 2000)

In the right panel in Fig. 6, the quartic coupling λ exhibits a Z_2 symmetry $\lambda \to -\lambda$ because it enters the Higgs and DM observables only through λ^2. Most of these points also fall within the range $m_{H^\pm} \in [110, 120]$ GeV. The yellow points are predominantly in the negative λ region owing to the collective influence of parameters, such as M_1, μ, and μ_T, rather than a direct effect of λ itself. As λ decreases, the density of points with $m_h < 110$ GeV increases, reflecting the interplay of λ, μ, and μ_T in the expression for m_h (Eq. (10)). The red points favor the negative region of λ. Notably, some red points lie within the theoretically predicted green band to match the 95 GeV Higgs requirement.

Finally, in Fig. 7, the cyan points satisfying the Higgs constraints are diffusely distributed, showing no significant correlation with μ or μ_T. This indicates that the Higgs constraints impose relatively weak limits on these mass parameters. The yellow points, which satisfy the DM constraints, depend on the higgsino mass parameter μ, with their density increasing as μ increases. This occurs because the bino can become the LSP and achieve the correct relic density only for larger μ. The red points constrained by $\mu_{\gamma\gamma}$ and $\mu_{b\bar{b}}$ show a linear correlation with μ and μ_T, forming a narrow band near the TeV scale. This narrow band results from the cancellation between these

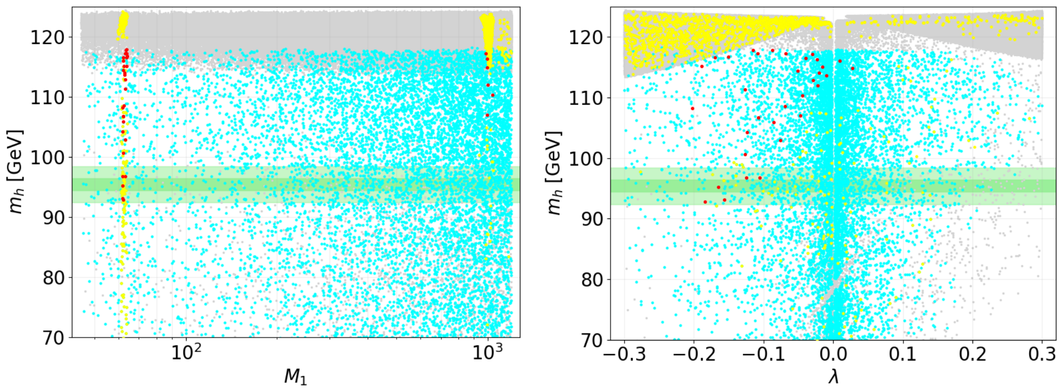

Fig. 6. (color online) Scanning results using the parameter ranges in Table 2. The left panel displays the relationship between the light scalar Higgs boson mass m_h and M_1, whereas the right panel presents the correlation between m_h and λ. The color scheme follows the description in the color conditions and the surrounding context. The green band represents $m_h = 95.4 \pm 1$ GeV, and the light green area represents $m_h = 95.4 \pm 3$ GeV.

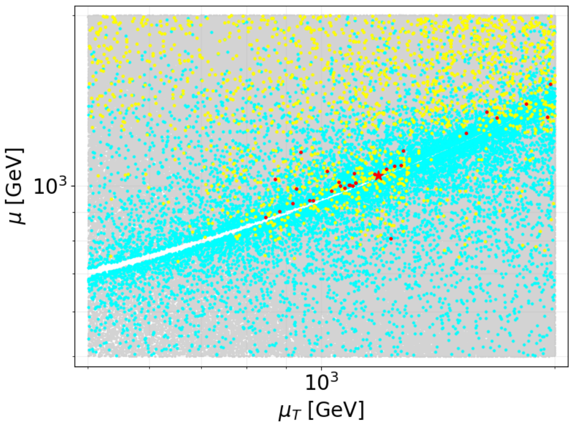

Fig. 7. (color online) Results of the global scan presented in the $\mu - \mu_T$ plane. The parameter points follow the color scheme described in the text. The red star markers represent the parameter sets satisfying all red point conditions plus the Higgs mass constraint $m_h = 95.4 \pm 1$ GeV.

mass parameters, consistent with Fig. 1 and Eq. (10). The jagged white regions represent the parameter space where the triplino is the next-to-lightest stable particle, consistent with Fig. 5.

V. CONCLUSIONS

This study systematically explored the TMSSM to explain the 95 GeV Higgs boson diphoton excess observed by CMS and ATLAS and its implications for DM physics. By incorporating an $SU(2)_L$ triplet superfield, the TMSSM reduces the fine-tuning issues of the MSSM and naturally supports Higgs boson masses at 95 GeV and 125 GeV. Our calculations show that optimizing triplet-doublet mixing and parameters λ and μ_T enables the TMSSM to reproduce the experimental diphoton signal strength, $\mu_{\gamma\gamma}^{\rm CMS+ATLAS} = 0.24^{+0.09}_{-0.08}$. The model reproduces the LEP $b\bar{b}$ excess with $\mu_{b\bar{b}} = 0.117 \pm 0.057$, remaining compatible within 2σ in our scan. In the DM sector, the triplet and its supersymmetric partner, the triplino, enhance neutralino annihilation through Higgs resonance and co-annihilation, achieving consistency with the Planck-2018 cold DM relic density, $\Omega h^2 = 0.120 \pm 0.024$, while meeting direct and indirect detection constraints.

Using tools, such as SARAH, SPheno, MicrOmegas, and BSMArts, we performed a comprehensive scan of the TMSSM parameter space, identifying regions that simultaneously satisfy Higgs masses, $m_h \approx 95.4 \pm 1$ GeV and $m_H \approx 125 \pm 2$ GeV, both the diphoton and $b\bar{b}$ signal strengths within the 2σ level, and DM relic density requirements. These findings confirm that the TMSSM robustly explains the 95 GeV diphoton excess and the LEP $b\bar{b}$ excess and provides a consistent framework for DM physics. Future collider experiments, such as the High-Luminosity LHC or a next-generation circular collider, will precisely probe triplino properties and the 95 GeV Higgs signal, offering critical tests of the TMSSM and deeper insights into supersymmetric physics.

ACKNOWLEDGMENTS

We thank Mark Goodsell and Andreas Crivellin for the helpful discussions.

References

[1] L. Randall and R. Sundrum, Phys. Rev. Lett. **83**, 3370 (1999)

[2] N. Arkani-Hamed, S. Dimopoulos, and G. R. Dvali, Phys. Lett. B **429**, 263 (1998)

[3] H. E. Haber and G. L. Kane, Phys. Rept. **117**, 75 (1985)

[4] S. P. Martin, Adv. Ser. Direct. High Energy Phys. **18**, 1

(1998)
[5] G. Jungman, M. Kamionkowski, and K. Griest, Phys. Rept. **267**, 195 (1996)
[6] G. H. Duan, W. Wang, L. Wu *et al*., Phys. Lett. B **778**, 296 (2018)
[7] A. Hayrapetyan *et al*. (CMS), Phys. Rev. D **109**, 072007 (2024)
[8] G. Aad *et al*. (ATLAS), Phys. Rept. **1116**, 261 (2025)
[9] N. Craig, A. Katz, M. Strassler *et al*., JHEP **07**, 105 (2015)
[10] J. R. Espinosa and M. Quiros, Nucl. Phys. B **384**, 113 (1992)
[11] S. Di Chiara and K. Hsieh, Phys. Rev. D **78**, 055016 (2008)
[12] T. Basak and S. Mohanty, Phys. Rev. D **86**, 075031 (2012)
[13] L. Cort, M. Garcia, and M. Quiros, Phys. Rev. D **88**, 075010 (2013)
[14] P. Bandyopadhyay, K. Huitu, and A. Sabanci, JHEP **10**, 091 (2013)
[15] P. Bandyopadhyay, S. Di Chiara, K. Huitu *et al*., JHEP **11**, 062 (2014)
[16] M. Garcia-Pepin, S. Gori, M. Quiros *et al*., Phys. Rev. D **91**, 015016 (2015)
[17] P. Bandyopadhyay, C. Coriano, and A. Costantini, JHEP **09**, 045 (2015)
[18] P. Bandyopadhyay, C. Corianò, and A. Costantini, Phys. Rev. D **94**, 055030 (2016)
[19] P. Bandyopadhyay, C. Coriano, and A. Costantini, JHEP **12**, 127 (2015)
[20] J. L. Diaz-Cruz, J. Hernandez-Sanchez, S. Moretti *et al*., Phys. Rev. D **77**, 035007 (2008)
[21] C. Arina, V. Martin-Lozano, and G. Nardini, JHEP **08**, 015 (2014)
[22] E. Barradas-Guevara, O. Felix-Beltran, and A. Rosado, Phys. Rev. D **71**, 073004 (2005)
[23] M. Das, S. Di Chiara, and S. Roy, Phys. Rev. D **91**, 055013 (2015)
[24] P. Fileviez Perez and M. B. Wise, Phys. Rev. D **84**, 055015 (2011)
[25] A. M. Sirunyan *et al*. (CMS), Phys. Lett. B **793**, 320 (2019)
[26] CMS Collaboration (CMS), CMS-PAS-HIG-20-002 (2018), *Search for a standard model-like Higgs boson in the mass range between 70 and 110 GeV in the diphoton final state in proton-proton collisions at* $\sqrt{s}$ *= 13 TeV*
[27] ATLAS Collaboration (ATLAS), ATLAS-CONF-2018-025 (2018), *Search for resonances in the 65 to 110 GeV diphoton invariant mass range using 80* fb^{-1} *of pp collisions collected at* $\sqrt{s}$ *= 13 TeV with the ATLAS detector*
[28] ATLAS Collaboration (ATLAS), ATLAS-CONF-2023-035 (2023), *Search for diphoton resonances in the 66 to 110 GeV mass range using 140* fb^{-1} *of 13 TeV pp collisions collected with the ATLAS detector*
[29] T. Biekötter, S. Heinemeyer, and G. Weiglein, Phys. Rev. D **109**, 035005 (2024)
[30] R. Barate *et al*. (LEP Working Group for Higgs boson searches, ALEPH, DELPHI, L3, OPAL), Phys. Lett. B **565**, 61 (2003)
[31] J. Cao, X. Guo, Y. He *et al*., Phys. Rev. D **95**, 116001 (2017)
[32] A. Crivellin, J. Heeck, and D. Müller, Phys. Rev. D **97**, 035008 (2018)
[33] U. Haisch and A. Malinauskas, JHEP **03**, 135 (2018)
[34] P. J. Fox and N. Weiner, JHEP **08**, 025 (2018)
[35] D. Liu, J. Liu, C. E. M. Wagner *et al*., JHEP **06**, 150 (2018)
[36] K. Wang, F. Wang, J. Zhu *et al*., Chin. Phys. C **42**, 103109 (2018)
[37] L. Liu, H. Qiao, K. Wang *et al*., Chin. Phys. C **43**, 023104 (2019)
[38] T. Biekötter, M. Chakraborti, and S. Heinemeyer, Eur. Phys. J. C **80**, 2 (2020)
[39] J. M. Cline and T. Toma, Phys. Rev. D **100**, 035023 (2019)
[40] K. Choi, S. H. Im, K. S. Jeong *et al*., Eur. Phys. J. C **79**, 956 (2019)
[41] A. Kundu, S. Maharana, and P. Mondal, Nucl. Phys. B **955**, 115057 (2020)
[42] J. Cao, X. Jia, Y. Yue *et al*., Phys. Rev. D **101**, 055008 (2020)
[43] T. Biekötter, M. Chakraborti, and S. Heinemeyer, Int. J. Mod. Phys. A **36**, 2142018 (2021)
[44] A. A. Abdelalim, B. Das, S. Khalil *et al*., Nucl. Phys. B **985**, 116013 (2022)
[45] S. Heinemeyer, C. Li, F. Lika *et al*., Phys. Rev. D **106**, 075003 (2022)
[46] T. Biekötter, S. Heinemeyer, and G. Weiglein, JHEP **08**, 201 (2022)
[47] S. Iguro, T. Kitahara, and Y. Omura, Eur. Phys. J. C **82**, 1053 (2022)
[48] W. Li, H. Qiao, and J. Zhu, Chin. Phys. C **47**, 123102 (2023)
[49] T. Biekötter, S. Heinemeyer, and G. Weiglein, Phys. Lett. B **846**, 138217 (2023)
[50] C. Bonilla, A. E. Carcamo Hernandez, S. Kovalenko *et al*., JHEP **12**, 075 (2023)
[51] D. Azevedo, T. Biekötter, and P. M. Ferreira, JHEP **11**, 017 (2023)
[52] P. Escribano, V. M. Lozano, and A. Vicente, Phys. Rev. D **108**, 115001 (2023)
[53] A. Belyaev, R. Benbrik, M. Boukidi *et al*., JHEP **05**, 209 (2024)
[54] S. Ashanujjaman, S. Banik, G. Coloretti *et al*., Phys. Rev. D **108**, L091704 (2023)
[55] S. Baek, P. Ko, Y. Omura *et al*., Eur. Phys. J. C **85**, 908 (2025)
[56] X. Du, H. Liu, and Q. Chang, Phys. Rev. D **112**, 015019 (2025)
[57] S. Yaser Ayazi, M. Hosseini, S. Paktinat Mehdiabadi *et al*., Phys. Rev. D **110**, 055004 (2024)
[58] D. Borah, S. Mahapatra, P. K. Paul, *et al*., Phys. Rev. D **109**, 055021 (2024)
[59] S. Bhattacharya, G. Coloretti, A. Crivellin *et al*., (2023), arXiv: 2306.17209 [hep-ph]
[60] G. Coloretti, A. Crivellin, and B. Mellado, Phys. Rev. D **110**, 073001 (2024)
[61] S. Banik, G. Coloretti, A. Crivellin *et al*., JHEP **01**, 155 (2025)
[62] S. Ashanujjaman, S. Banik, G. Coloretti, *et al*., JHEP **04**, 003 (2025)
[63] P. S. B. Dev, R. N. Mohapatra, and Y. Zhang, Phys. Lett. B **849**, 138481 (2024)
[64] T. Mondal, S. Moretti, and P. Sanyal, (2024), arXiv: 2412.00474 [hep-ph]
[65] H. Xu, Y. Wang, X.-F. Han *et al*., (2025), arXiv: 2505.03592 [hep-ph]
[66] J. Cao, X. Jia, J. Lian *et al*., Phys. Rev. D **109**, 075001 (2024)
[67] U. Ellwanger and C. Hugonie, Eur. Phys. J. C **83**, 1138 (2023)

[68] J. Lian, Phys. Rev. D **110**, 115018 (2024)
[69] U. Ellwanger, C. Hugonie, S. F. King *et al.*, Eur. Phys. J. C **84**, 788 (2024)
[70] U. Ellwanger and C. Hugonie, Eur. Phys. J. C **84**, 526 (2024)
[71] J. Cao, X. Jia, and J. Lian, Phys. Rev. D **110**, 115039 (2024)
[72] C.-X. Liu, Y. Zhou, X.-Y. Zheng *et al.*, Phys. Rev. D **109**, 056001 (2024)
[73] G. Belanger, U. Ellwanger, J. F. Gunion *et al.*, JHEP **01**, 069 (2013)
[74] T. Biekötter, S. Heinemeyer, and C. Muñoz, Eur. Phys. J. C **78**, 504 (2018)
[75] F. Domingo, S. Heinemeyer, S. Paßehr *et al.*, Eur. Phys. J. C **78**, 942 (2018)
[76] W. G. Hollik, S. Liebler, G. Moortgat-Pick *et al.*, Eur. Phys. J. C **79**, 75 (2019)
[77] W. G. Hollik, C. Li, G. Moortgat-Pick *et al.*, Eur. Phys. J. C **81**, 141 (2021)
[78] T. Biekötter, A. Grohsjean, S. Heinemeyer *et al.*, Eur. Phys. J. C **82**, 178 (2022)
[79] A. Adhikary, R. K. Barman, B. Bhattacherjee *et al.*, Phys. Rev. D **108**, 035020 (2023)
[80] W. Li, H. Qiao, K. Wang *et al.*, (2023), arXiv: 2312.17599 [hep-ph]
[81] S. Roy and C. E. M. Wagner, JHEP **04**, 106 (2024)
[82] J. Edsjo and P. Gondolo, Phys. Rev. D **56**, 1879 (1997)
[83] A. Delgado, M. Garcia-Pepin, B. Ostdiek *et al.*, Phys. Rev. D **92**, 015011 (2015)
[84] A. Djouadi, Phys. Rept. **459**, 1 (2008)
[85] J. A. Evans, A. Ghalsasi, S. Gori *et al.*, JHEP **02**, 151 (2020)
[86] G. Belanger, F. Boudjema, A. Pukhov *et al.*, Comput. Phys. Commun. **176**, 367 (2007)
[87] G. Belanger, F. Boudjema, A. Pukhov *et al.*, Comput. Phys. Commun. **180**, 747 (2009)
[88] G. Belanger, F. Boudjema, A. Pukhov *et al.*, Nuovo Cim. C **033N2**, 111 (2010)
[89] G. Belanger, F. Boudjema, A. Pukhov *et al.*, Comput. Phys. Commun. **185**, 960 (2014)
[90] G. Bélanger, F. Boudjema, A. Pukhov *et al.*, Comput. Phys. Commun. **192**, 322 (2015)
[91] G. Bélanger, F. Boudjema, A. Goudelis *et al.*, Comput. Phys. Commun. **231**, 173 (2018)
[92] M. Abdughani, L. Wu, and J. M. Yang, Eur. Phys. J. C **78**, 4 (2018)
[93] G. H. Duan, K.-I. Hikasa, J. Ren *et al.*, Phys. Rev. D **98**, 015010 (2018)
[94] M. Abdughani and L. Wu, Eur. Phys. J. C **80**, 233 (2020)
[95] G. H. Duan, C. Han, B. Peng *et al.*, Phys. Lett. B **788**, 475 (2019)
[96] N. Arkani-Hamed, A. Delgado, and G. F. Giudice, Nucl. Phys. B **741**, 108 (2006)
[97] Z.-J. Yang, J.-L. Yang, S.-M. Zhao *et al.*, Eur. Phys. J. C **84**, 1216 (2024)
[98] C. Cheung, L. J. Hall, D. Pinner *et al.*, JHEP **05**, 100 (2013)
[99] T. Basak and S. Mohanty, JHEP **08**, 020 (2013)
[100] J. R. Ellis, A. Ferstl, and K. A. Olive, Phys. Lett. B **481**, 304 (2000)
[101] F. Staub, (2008), arXiv: 0806.0538 [hep-ph]
[102] W. Porod, Comput. Phys. Commun. **153**, 275 (2003)
[103] W. Porod and F. Staub, Comput. Phys. Commun. **183**, 2458 (2012)
[104] H. Bahl, T. Biekötter, S. Heinemeyer *et al.*, Comput. Phys. Commun. **291**, 108803 (2023)
[105] P. Bechtle, O. Brein, S. Heinemeyer *et al.*, Comput. Phys. Commun. **181**, 138 (2010)
[106] P. Bechtle, O. Brein, S. Heinemeyer *et al.*, Comput. Phys. Commun. **182**, 2605 (2011)
[107] P. Bechtle, O. Brein, S. Heinemeyer *et al.*, PoS **CHARGED2012**, 024 (2012)
[108] P. Bechtle, O. Brein, S. Heinemeyer *et al.*, Eur. Phys. J. C **74**, 2693 (2014)
[109] P. Bechtle, S. Heinemeyer, O. Stal *et al.*, Eur. Phys. J. C **75**, 421 (2015)
[110] P. Bechtle, D. Dercks, S. Heinemeyer *et al.*, Eur. Phys. J. C **80**, 1211 (2020)
[111] H. Bahl, V. M. Lozano, T. Stefaniak *et al.*, Eur. Phys. J. C **82**, 584 (2022)
[112] P. Bechtle, S. Heinemeyer, O. Stål *et al.*, Eur. Phys. J. C **74**, 2711 (2014)
[113] O. Stål and T. Stefaniak, PoS **EPS-HEP2013**, 314 (2013)
[114] P. Bechtle, S. Heinemeyer, O. Stål *et al.*, JHEP **11**, 039 (2014)
[115] P. Bechtle, S. Heinemeyer, T. Klingl *et al.*, Eur. Phys. J. C **81**, 145 (2021)
[116] M. M. Altakach, S. Kraml, A. Lessa *et al.*, JHEP **11**, 074 (2024)
[117] M. D. Goodsell and A. Joury, Comput. Phys. Commun. **297**, 109057 (2024)
[118] A. E. Faraggi and M. D. Goodsell, Eur. Phys. J. C **84**, 589 (2024)
[119] B. Fuks, M. D. Goodsell, and T. Murphy, Phys. Rev. D **111**, 055010 (2025)
[120] D. Agin, B. Fuks, M. D. Goodsell *et al.*, Phys. Lett. B **853**, 138597 (2024)
[121] D. Agin, B. Fuks, M. D. Goodsell *et al.*, Eur. Phys. J. C **84**, 1218 (2024)
[122] K. Benakli, M. Goodsell, W. Ke *et al.*, Eur. Phys. J. C **83**, 43 (2023)
[123] M. D. Goodsell and A. Joury, Eur. Phys. J. C **83**, 268 (2023)
[124] M. D. Goodsell and L. Priya, Eur. Phys. J. C **82**, 235 (2022)
[125] M. D. Goodsell and R. Moutafis, Eur. Phys. J. C **81**, 808 (2021)
[126] G. Domènech, M. Goodsell, and C. Wetterich, JHEP **01**, 180 (2021)
[127] F. Feroz and M. P. Hobson, Mon. Not. Roy. Astron. Soc. **384**, 449 (2008)
[128] F. Feroz, M. P. Hobson, and M. Bridges, Mon. Not. Roy. Astron. Soc. **398**, 1601 (2009)
[129] F. Feroz, M. P. Hobson, E. Cameron *et al.*, Open J. Astrophys. **2**, 10 (2019)
[130] M. D. Goodsell, K. Nickel, and F. Staub, Eur. Phys. J. C **75**, 32 (2015)
[131] M. Goodsell, K. Nickel, and F. Staub, Eur. Phys. J. C **75**, 290 (2015)
[132] N. Aghanim *et al.* (Planck), Astron. Astrophys. **641**, A6 (2020)